Hindawi
Geofluids
Volume 2022, Article ID 6914746, 17 pages
https://doi.org/10.1155/2022/6914746

Research Article

Structural Characteristics of Regenerated Roof and Distribution Law of Overburden Porosity in Downward Mining of a Bifurcated Coal Seam

Ru Hu,[1,2] **Jiwen Wu**,[2] **Xiaorong Zhai**,[2] **Wenbao Shi**,[3] **and Kai Huang**[2]

[1]*State Key Laboratory of Mining Response and Disaster Prevention and Control in Deep Coal Mines, Anhui University of Science and Technology, Huainan 232001, China*
[2]*School of Earth and Environment, Anhui University of Science and Technology, Huainan 232001, China*
[3]*School of Mining Engineering, Anhui University of Science and Technology, Huainan 232001, China*

Correspondence should be addressed to Xiaorong Zhai; 616170984@qq.com

Received 15 October 2021; Revised 10 November 2021; Accepted 25 February 2022; Published 19 March 2022

Academic Editor: Yong-Zheng Wu

During downward mining of a bifurcated coal seam, the roof of the lower coal seam is relatively broken and difficult to control due to the mining influence of the upper coal seam. Roof accidents occur frequently during mining of the lower coal seam, reducing mining efficiency. How to ensure safe and efficient mining of the lower coal seam is a significant issue. In this paper, overlying strata migration and fracture characteristics of the lower coal seam, the structure and stability of the regenerated roof, and porosity and permeability characteristics of the overlying strata under the mining influence of the upper coal seam are studied by using similar simulation tests. Results show that the overburden structure of the lower coal seam is altered due to the mining influence of the upper coal seam, and the regenerated roof of the lower coal seam is divided into three structural types from top to bottom, namely: intact rock mass+block fracture rock mass+loose rock mass (type I structure); intact rock mass+block fracture rock mass+loose rock mass+cataclastic rock mass (type II structure); and intact rock mass+block fracture rock mass+loose rock mass+cataclastic rock mass+slab-rent rock mass (type III structure). The stability of each type of rock mass structure is evaluated, and the stability of three types of rock mass structures is III > II > I. The overburden porosity and slurry permeability coefficient are relatively large at the cutting hole and stopping line. The porosity of the caving zone within 70 m of the cut hole and stopping line is greater than 5%, and the permeability coefficient is greater than 0.1 m/s. Based on differences in the surrounding rock porosity and permeability characteristics, the grouting difficulty of overburden is divided into three types of areas: extremely easy grouting areas, easy grouting areas, and difficult grouting areas. The results of this paper can provide reference for the stability evaluation of the regenerated roof and the selection of grouting treatment parameters for the broken roof under similar conditions.

1. Introduction

In China, there are many reserves and wide distribution of coal resources under the condition of close storage [1, 2]. In recent years, with the depletion of easily mined coal resources, more and more close-distance coal seams with complex conditions are being mined. Bifurcated coal seams are one type of close-distance coal seam. Due to differences in interlayer thickness, the selection of mining technology for use in bifurcated coal seam stopes can be problematic, especially during layered mining of a coal seam in a bifurcated area, in which the roof of the lower coal seam is broken and difficult to control due to the mining influence of the upper coal seam, which seriously affects the safety and production efficiency of the working face [3–5]. Therefore, ensuring the safe mining of the lower coal seam is the primary concern when mining bifurcated coal seams.

Numerous scholars have conducted systematic research on the deformation and failure of rock surrounding a short-range coal seam stope [6–9], the distribution of stope spatial

abutment pressure [10–15], roadway layout and support [16–20], and the stability of surrounding rock support [21–23], which has improved short-range coal seam mining theory and significantly improved the recovery rate of coal resources. However, there are few relevant studies on the stope of bifurcated coal seams as well as a lack of systematic research on the structural changes of the regenerated roof of the lower coal seam due to the mining influence. Mastering the structural characteristics of the regenerated roof is critical for effective treatment of the regenerated roof. At present, multiple effective and scientific technical treatment methods have been proposed for the broken roof, among which grouting reinforcement technology is primarily used for the treatment of broken rock mass [24–29]. Whether underground or surface grouting, for the whole grouting target area, the selection of grouting parameters is commonly based on production experience, without considering difference in the porosity and permeability of grouting target area caused by different overburden structures after mining. Such a lack of consideration may lead to grouting omission or material waste. Existing theoretical studies show that there are significant differences in porosity and permeability at different positions within overburden. Numerous scholars have conducted research regarding the porosity and permeability evolution of overburden. Adhikary and Guo et al. used a numerical simulation to calculate formation permeability due to the mining influence, producing results that are highly consistent with field test data [30]. Zhang et al. studied the compaction characteristics of the goaf caving zone, revealed the primary factors affecting the compaction process of the caving zone, and accurately calculated the compaction degree of the goaf using various methods [31]. Poulsen et al. proposed a numerical model to express the overburden fracture process induced by mining and estimated the permeability of overburden using the Kozeny-Carman permeability-porosity equation [32]. Ma et al. systematically studied the mechanical behavior and failure mechanism of rock mass in deep rock engineering and analyzed the hydraulic properties and deformation behavior of filling materials in filling mining through laboratory tests [33–36]. Existing research primarily focuses on water seepage within the overburden, goaf ventilation design, gas discharge, and natural ignition of the goaf [37–39]. Unfortunately, there are few studies on using differences in overburden porosity and permeability characteristics to guide the grouting of the broken roof. For coal seam stopes, current research methods primarily include similarity simulation [40, 41], numerical simulation [42, 43], field test [44–47], engineering analogy [48], theoretical analysis [49–51], and empirical formula calculation [52–54]. In terms of accuracy, field test results are more accurate, but field test implementation is difficult and costly. In contrast, simulations are easy to operate, low-cost, and accurate enough to meet production needs, making simulations more common than field studies. Most similar simulation tests are carried out around a single coal seam and close-distance coal seam stope. Few relevant studies on the mining conditions of bifurcated coal seams exist.

Based on the above analysis, this paper examines the bifurcated close coal seams in the Xutuan mining area of Anhui Province, specifically analyzing the regenerated roof of the lower coal seam. Through similar simulation experiments, this paper studies the deformation and fracturing of the surrounding rock during mining of the upper coal seam, divides the structural types of the regenerated roof, and analyzes the stability of different structural types of the regenerated roof during mining of the lower coal seam. According to differences in overburden porosity and permeability, the difficulty of grouting in the treatment area of the regenerated roof is determined, in order to provide a basis for the selection of grouting parameters for the broken roof in the lower coal seam.

2. Geological Overview of the Study Area

The no. 7 coal seam in the Xutuan mining area is the primary coal seam of the mine. The study area for this paper is located at the 72210 working face and the upper 71212 working face in the eighth mining area of the mine. The no. 7-1 and no. 7-2 coal seams are bifurcated and merged. The distance between the two coal seams is 0.7 m~9.0 m, with an average of 5.8 m. The spatial positions of no. 7-1 and no. 7-2 coal seams are shown in Figure 1.

The elevation of the 71212 working face is -500.0 m~-571.2 m, the strike length of the working face is 1366 m, and the inclined width is 168 m. The elevation of the 71212 working face is -500.0 m~-571.2 m, the strike length of the working face is 1366 m, the inclined width is 168 m, and the average thickness of the coal seam is 2 m. Strike long-arm mining is used to excavate coal seams. The elevation of the 72210 working face is -486.0 m~-593.5 m, the strike length of the working face is 2023 m, the inclined width is 184 m, and the average thickness of the coal seam is 3 m. The burial depth of the no. 7-1 coal seam in the study area is 550 m, and the thickness of the coal seam is 2 m. The dip angle of the no.7-2 coal seam along the strike profile is subhorizontal, and the dip angle of the no. 7-2 coal seam is 5°. For the in situ stress field in the study area, the maximum principal stress σ_1, minimum principal stress σ_3, and intermediate principal stress σ_2 are 13.51 MPa, 7.52 MPa, and 8.93 MPa, respectively. The included angle between the maximum principal stress direction and the vertical direction is about 23°, the direction of the minimum principal stress is consistent with the rock stratum trend, the direction of the middle principal stress is perpendicular to σ_1, and the maximum principal stress is about equal to the self-weight stress of the overburden. The plane layout of the working face is shown in Figure 2.

3. Simulation of Similar Materials in a Bifurcated Coal Seam Stope

The geological environment of the working face is complex, field tests are difficult to conduct, and the transportation of equipment and materials is difficult. According to similarity theory, the similarity transformation of the geological environment of the working face and the indoor similarity simulation test can not only achieve the research purpose but also are low-cost, which has become an important research means [55, 56].

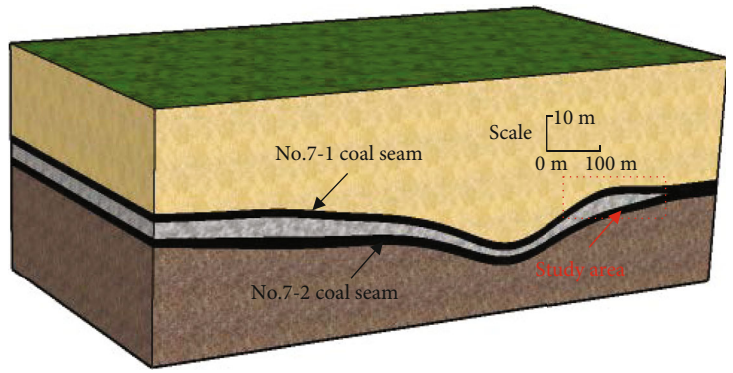

Figure 1: Schematic diagram of the no. 7-1 and no. 7-2 coal seams.

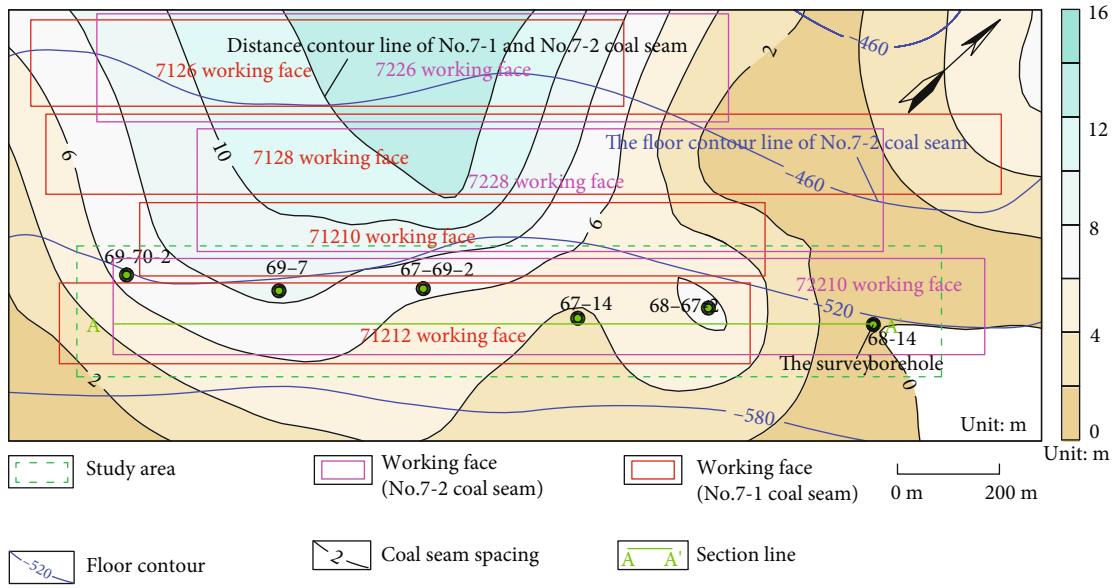

Figure 2: Plane layout of the working face.

3.1. Selection of Similar Simulation Test Parameters. According to the similarity principle, the selection of the similarity constant of the model is shown in Table 1(Table 1 is reproduced from Hu et al.) [40]. Combined with mechanical test results of the roof and floor rock mass of the working face, the material ratio orthogonal test can be carried out to determine the mechanical strength and ratio number of the model material. The detailed parameters and ratios are shown in Table 2.

The size of the similar model is 300 cm × 30 cm × 150 cm (length × width × height). In the process of model laying, the stress sensor (BW micro pressure box) is embedded and connected to the static resistance strain gauge (YJZA-32), the micro strain of overburden in the process of coal seam mining is obtained, and then the stress is further calculated through the formula, so as to achieve the purpose of stress monitoring. The conversion formula of stress and strain is as follows:

$$P = \mu\varepsilon \times K. \quad (1)$$

In formula (1), P is the pressure value (unit: KPa), $\mu\varepsilon$ is the strain, and K is the calibration coefficient (measured before delivery). The model and survey line layout are shown in Figure 3.

GetData Graph Digitizer software is used to postprocess the photos and extract the coordinate values of overburden displacement measuring points. Firstly, import the picture into the software, select O and A points that are not affected by mining horizontally as the x-axis control points, and O and A points are at the same horizontal line. Two points O and B in the vertical direction are selected as the y-axis control points, and the two points O and B are in the same vertical line. The three basic control points remain unchanged in each photo, and a two-dimensional plane coordinate system is established (Figure 4(a)). Secondly, the initial coordinate values of each displacement measuring point of overburden are obtained in the constructed two-dimensional coordinate system (Figure 4(b)). Finally, the coordinate values of overburden displacement measuring points during coal seam excavation are extracted and compared with the initial coordinate values to obtain the

Table 1: List of similar constants of the model.

Similarity constant	Model	Original rock
Similarity geometric ratio	1	100
Similarity bulk density ratio	0.608	1
Similarity elastic modulus ratio	0.00608	1
Similarity strength ratio	0.00608	1
Similarity Poisson ratio	1	1
Similarity time ratio	1	10

subsidence value of overburden (Figure 4(c)). During coal seam excavation, the displacement and stress of surrounding rock are monitored.

3.2. Analysis on Deformation and Failure Characteristics of Rock Mass in Upper Coal Seam Mining. When the working face advances to 90 m, the development heights of the caving zone and the fracture zone are 4.5 m and 19.3 m, respectively. The fracture angles of the overlying rock at the cut and the end of the working face are 54° and 49°, respectively. The surrounding rock of the stope forms an asymmetric trapezoidal failure mode along the fracture line. The overburden structure evolves from the original layered structure to the granular structure of the caving zone and fractured structure of the fracture zone (Figure 5(a)). When the working face advances to 165 m, affected by tectonic fissures in front of the working face, the overlying strata of the no.7–1 coal seam collapse along the tectonic fissure. A large crack appears at 19.5 m of the roof, and the crack width is about 1 m. Due to the rapid subsidence of the collapsed rock mass, the integrity is high, and the height of the caving zone is stable at 7.5 m. The maximum height of the fracture zone is 30.7 m. Thus far, the height of the two zones is stable (Figure 5(b)). When the working face advances to 220 m, mining of the 7-1 coal seam is completed, and the overburden fracture shape of the stope reaches a stable state. Due to the influence of tectonic fissures, compared with the degree of overburden fracture in front of tectonic fissure, after the coal seam pushes through tectonic fissure, and the overburden migration and fracture, the structure is obviously loose, the damage is more intense, and the pores are obviously large. The height of the collapse zone is 8 m, and the development height of the fracture zone is about 37 m (Figure 5(c)).

3.3. Stress Evolution Law of Roof and Floor Rock Mass. As the working face advances, the monitoring data at each measuring point on roof stress measuring line (monitoring line B) are recorded (Figure 6).

Monitoring line B is located 8 m from the roof of the no. 7-1 coal seam. Measuring point B5 shows the change in roof stress during advancement of the working face. During the advancing process, a stress concentration appeared in front of the coal wall, and the abutment pressure increased significantly. The influence range of the advance stress was 40 m–50 m, and the peak position of the abutment pressure was approximately 10 m away from the coal wall of the working face. When the working face passes through the measuring point, the roof is in a state of pressure relief, and the stress value decreases rapidly. As the overburden rock breaks and falls, it is gradually compacted, and the stress on rock mass in the upper part of the goaf is gradually restored. The stress recovery distance of the stress measuring point near the middle of the working face is 70 m~90 m as the working face advances (Figure 6). The stress value is stable 80 m away from the measuring point and is always slightly less than the original rock stress. The average breaking distance of the rock stratum is approximately 20 m. As stress increases, the fractured rock mass is gradually compacted, and the crack is closed (Figure 7).

The external reflection of overburden stress recovery is the compaction and closure of pores and fractures. When the working face advances to 90 m, transverse cracks appear behind the B4 measuring point. The stress value decreases rapidly to 0.0037 MPa after the working face passes the B4 measuring point (Figure 7). When advancing to 130 m, the stress value at B4 recovers to 0.0565 MPa, and the crack opening decreases significantly. When advancing to 170 m, the stress value of the measuring point is restored to 0.0641 MPa, which is close to the original rock stress value of 0.0822 MPa. With continuous advancement of the working face, the fracture opening closes and is stable. The roof stress recovery distance is 80 m, which is important for judging the compaction degree of the goaf rock mass and the boundary of stress zoning.

The C stress monitoring line is located at 28 m from the roof of the no. 7-1 coal seam. During the advancing process of the working face, the stress variation characteristics are consistent with those of survey line B (Figure 8). Next, take measuring point C3 as an example to illustrate the stress variation characteristics of rock mass in the fracture zone. Based on the stress recovery process of the C3 measuring point, the stress transmission is lagging; that is, after the fracture and migration of the overburden, the stress will not respond immediately but requires a certain transmission time. As the working face advances, the influence range of the advance abutment pressure in front of the working face is 40 m~50 m, and the peak position of abutment pressure is approximately 10 m from the coal wall of the working face. After the working face passes the stress measuring point 70 m~90 m, the stress is restored to the original rock stress.

The similar simulation test has difficulty observing the development of micro fractures in the model; therefore, the stress of the floor is primarily monitored during mining of the no. 7-1 coal seam. The failure depth of the No. 7-1 coal seam floor can be indirectly determined by analyzing the influence depth and transmission law of the floor stress. The monitoring data of A stress monitoring line are shown in Figure 9.

The A1~A5 sensor distance from the 7-1 coal seam is 1.75 m~8.75 m, and the A5 sensor distance from the no. 7-1 coal seam is 8.75 m. The stress change caused by 7-1 coal mining has obvious regularity in the transmission of the floor (Figure 9). With increasing burial depth, the variation trend line of peak stress peak at the A1~A10 stress sensors gradually becomes flat. When the distance between the stress sensor and the coal seam is greater than 8.75 m, the stress is

Table 2: Material parameters and mixing ratios.

Lithology	Original rock		Model					
	Stratum thickness (m)	Compressive strength (MPa)	Compressive strength (MPa)	Material ratio Sand : lime : gypsum	Weight of material (kg) Sand	Lime	Gypsum	Water
Mudstone	2.0	20.40	0.124	12 : 3 : 7	27.9	0.7	1.6	3.0
Siltstone	4.0	43.44	0.264	10 : 7 : 3	55.0	3.8	1.6	6.0
Mudstone	1.0	18.50	0.112	12 : 3 : 7	14.0	0.3	0.8	1.5
Fine sandstone	2.0	52.80	0.460	8 : 7 : 3	26.9	2.4	1.0	3.0
Mudstone	2.0	18.40	0.112	12 : 3 : 7	27.9	0.7	1.6	3.0
Siltstone	2.0	41.70	0.264	10 : 7 : 3	27.5	1.9	0.8	3.0
Mudstone	3.0	17.30	0.112	12 : 3 : 7	41.9	1.0	2.4	4.5
Fine sandstone	4.0	71.80	0.460	8 : 7 : 3	53.8	4.7	2.0	6.0
Siltstone	2.0	35.70	0.264	10 : 7 : 3	27.5	1.9	0.8	3.0
Mudstone	9.0	20.50	0.112	12 : 3 : 7	125.6	3.1	7.3	13.6
Fine sandstone	4.0	65.00	0.460	8 : 7 : 3	53.8	4.7	2.0	6.0
Mudstone	5.0	19.20	0.112	12 : 3 : 7	69.8	1.7	4.1	7.6
5-1 coal	2.0	6.50	0.038	13 : 4 : 6	28.1	0.9	1.3	3.0
Mudstone	6.0	17.50	0.112	12 : 3 : 7	83.7	2.1	4.9	9.1
5-2 coal	1.0	7.30	0.038	13 : 4 : 6	14.0	0.4	0.6	1.5
Mudstone	9.0	18.30	0.112	12 : 3 : 7	125.6	3.1	7.3	13.6
Siltstone	3.0	29.50	0.264	10 : 7 : 3	41.2	2.9	1.2	4.5
Fine sandstone	1.0	55.80	0.460	8 : 7 : 3	13.4	1.2	0.5	1.5
Mudstone	3.0	19.40	0.112	12 : 3 : 7	41.9	1.0	2.4	4.5
Fine sandstone	16.0	76.50	0.460	8 : 7 : 3	215.0	18.8	8.1	24.2
Siltstone	11.0	45.90	0.264	10 : 7 : 3	151.2	10.6	4.5	16.6
Mudstone	6.0	15.50	0.112	12 : 3 : 7	83.7	2.1	4.9	9.1
Fine sandstone	5.0	60.30	0.460	8 : 7 : 3	67.2	5.9	2.5	7.6
Mudstone	5.0	16.80	0.112	12 : 3 : 7	69.8	1.7	4.1	7.6
7-1 coal	2.0	8.20	0.038	13 : 4 : 6	28.1	0.9	1.3	3.0
Mudstone	0 ~ 23	18.40	0.112	12 : 3 : 7	137.6	3.4	8.0	14.9
7-2 coal	3.0	7.50	0.038	13 : 4 : 6	42.2	1.3	1.9	4.5
Mudstone	3.0	23.36	0.142	12 : 3 : 7	38.9	1.0	2.3	4.2
Fine sandstone	11.0	75.60	0.460	8 : 7 : 3	148.4	13.0	5.6	16.7
Mudstone	2.0	45.07	0.274	10 : 7 : 3	26.7	1.9	0.8	2.9
8-2 coal	3.0	8.60	0.407	8 : 7 : 3	35.3	3.1	1.3	4.0
Mudstone	4.0	28.50	0.192	12 : 3 : 7	41.1	1.1	2.6	4.5
Siltstone	2.0	39.70	0.274	10 : 7 : 3	17.2	1.2	0.5	1.9
Fine sandstone	4.0	66.80	0.407	8 : 7 : 3	27.5	2.4	1.0	3.1
Mudstone	4.0	31.57	0.192	12 : 3 : 7	20.0	0.5	1.2	2.2

not affected by the abutment pressure in front of the working face, and the variation range is small. The stress peak monitored by the A5 stress sensor is less than that of A4 measuring point, and its stress peak is at the inflection point of the stress peak trend line. Therefore, the range of the strong failure zone in the floor formed by the stress change caused by mining is 5.00 m~8.75 m. The strata in this range are severely damaged due to the strong rock pressure, forming fractures. The crack development depth is 6 m (Figure 10). The development height of "two zones" of overburden and the failure depth of the floor are measured in the study area, which verifies the reliability of similar simulation results [40].

During mining, the floor of the working face is affected by the advance abutment pressure and is in a supercharging state. When the goaf is formed, the floor rock mass undergoes a high degree of pressure relief. With periodic collapse and gradual compaction of overburden, the floor stress begins to increase gradually until it becomes stable; however, the restored stress value is always slightly less than the initial stress, and the stress recovery distance is 70 m~90 m.

3.4. Structural Type Division and Stability Analysis of the Regenerated Roof. The rock mass in the caving zone is loose and is classified as either granular rock mass or block

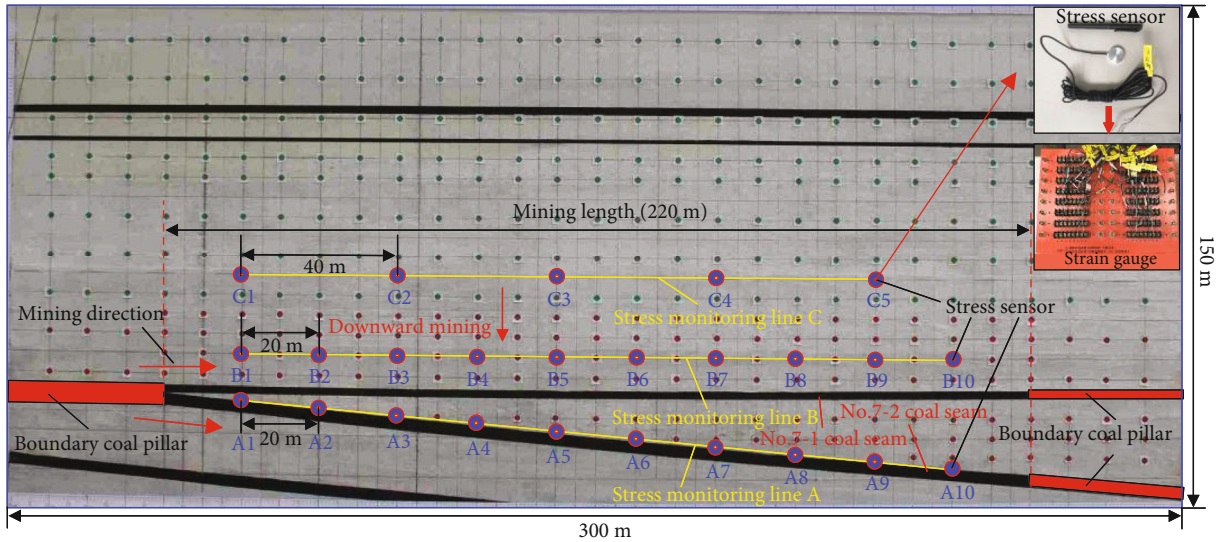

Figure 3: Schematic diagram of the monitoring line layout in the model.

fracture rock mass, which contains well-developed fractures. According to the stress transfer law of the floor, the floor is affected by mining forming a strong failure zone, and the rock mass in the strong failure zone is cut by mining fissures producing a cataclastic rock mass. The average depth of the strong failure zone of the floor is 6 m, and the rock mass in the lower part of the strong failure zone is less affected by mining (rock pressure disturbance zone), which can be considered staying in the original rock state and being a slab-rent rock mass. Based on the previous experience of mining bifurcated coal seams in the Xutuan coal mine as well as the results of similar simulation tests, when the coal seam spacing is less than 1 m, after mining the no. 7-1 coal seam, the top-down rock mass structure combination type of the no. 7-2 coal seam roof can be divided into intact rock mass+block fracture rock mass+loose rock mass (type I structure). When the coal seam spacing is between 1 m and 6 m, the rock mass structure combination type of the no. 7-2 coal seam roof can be divided into intact rock mass+block fracture rock mass+loose rock mass+cataclastic rock mass (type II structure). When the coal seam spacing is greater than 6 m, the rock mass structure combination type of the no. 7-2 coal seam roof can be divided into intact rock mass+block fracture rock mass+loose rock mass+cataclastic rock mass+slab-rent rock mass (type III structure) (Figure 11).

According to the above research results, the average failure depth of the strong failure zone of the floor of the no. 7-1 coal seam is 6 m. The stability of three regenerated roof structures is analyzed during mining of the no. 7-2 coal seam. The fracture form of roof rock mass when the no. 7-2 coal seam advances to 10 m, 50 m, and 70 m is shown in Figure 12.

When the working face advances to 10 m, the roof of coal seam 7-2 is directly covered with the caving zone of coal seam 7-1 (Figure 12(a)). During mining of the 7-2 coal seam, the loose rock mass in the caving zone of the no. 7-1 coal seam directly falls. Under the condition of this type of roof structure, the roof of the working face is relatively broken and difficult to control. Also, the roof leaks during mining, which poses a great threat to the safety of the working face. When the working face advances to 50 m, due to the gradual increase in interlayer distance, the interlayer strata of the no. 7-1 and 7-2 coal seams form a small-scale masonry beam structure, which plays a supporting role in the upper loose caving zone. As the mined area increases, the small-scale masonry beam structure rapidly becomes unstable, and the loose rock mass in the upper caving zone rapidly collapses (Figure 12(b)). When the working face advances to 70 m, the distance between the coal seams further increases, close to the depth (6 m) of the strong failure zone of the no. 7-1 coal seam floor, and the length of cantilever beam formed at the end of the working face gradually increases, which plays a significant supporting role for the upper rock stratum and prevents the downward movement of loose rock mass in the upper caving zone (Figure 12(c)). When the working face advances to 90 m, 165 m, and 220 m, the failure mode of surrounding rock is shown in Figure 13.

When the 7–2 coal seam advances to 90 m, the thickness of the interlayer rock at this position exceeded 6 m (Figure 13(a)). The cantilever beam structure formed at 70 m is broken and hinged with the collapsed rock mass behind it, forming a new masonry beam structure. With increasing thickness of the masonry beam structure, the breaking length of the rock mass increases significantly, and the stability of the masonry beam structure is enhanced. When the working face is advanced to 165 m, the length of the masonry beam continues to increase, and with increasing interlayer rock thickness, the thickness of masonry beam as well as the ultimate breaking distance of rock stratum at the end of the working face also increases, which will better support the upper rock mass before failure, which is conducive to successfully managing the working face roof (Figure 13(b)). When the working face advances to 220 m, with increasing interlayer distance, and when the interlayer thickness exceeds 6 m, the breaking length of cantilever rock

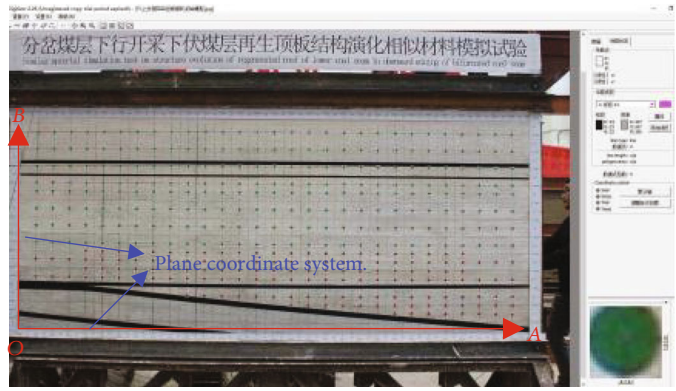

(a) Establish the two-dimensional plane coordinate system of the model

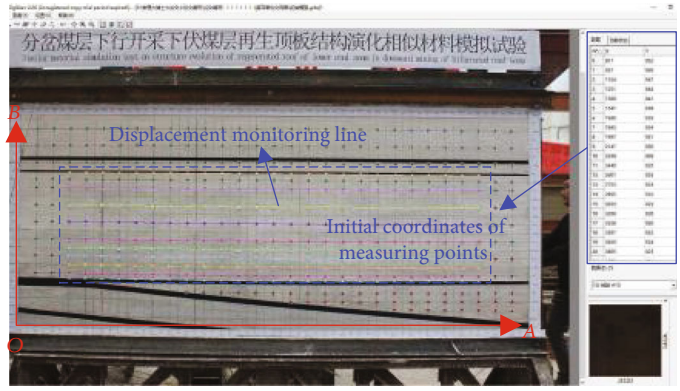

(b) Extract the initial coordinate value of the model measuring point

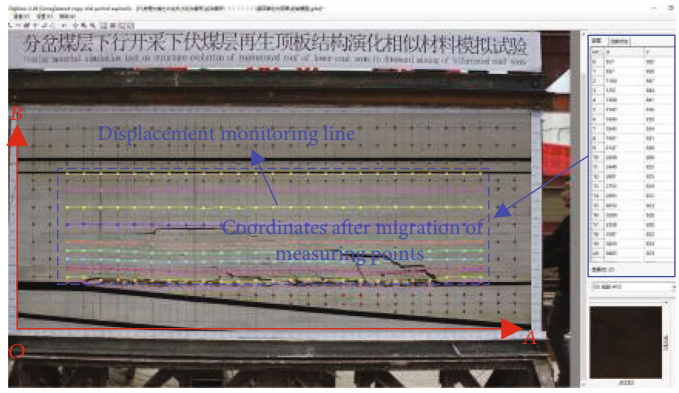

(c) Extract the coordinate values of measuring points after coal seam mining

Figure 4: Schematic diagram of measuring point displacement data extraction.

at the end of the working face gradually increases (Figure 13(c)). After breaking, they hinge with each other to form a masonry beam structure, so that mining of the no. 7-2 coal seam is not affected by mining of the no. 7-1 coal seam. In summary, when the coal seam spacing is less than 6 m, the rock mass structure of type I and type II roofs is relatively unstable, the interlayer structure is relatively loose, and the roof is broken, making it difficult to manage. When the interlayer distance is greater than 6 m, a stable masonry beam structure is formed between the layers, which can support the caving zone of the no. 7-1 coal seam. The stability of the three types of regenerated roof structure is III > II > I.

4. Study on Evolution Characteristics of Porosity and Permeability of Roof Overburden in the No. 7-2 Coal Seam

4.1. Distribution Characteristics of Porosity and Permeability Coefficient of Overburden. Through the analysis of the structural stability of various types of the regenerated roof, the rock mass structure of type I and II roofs is determined to be relatively unstable, and the interlayer structure is relatively loose, requiring that the broken rock mass be reinforced. The previous experience of mining the no. 7-2 coal seam in the Xutuan coal mine shows that when the coal seam spacing is less than 6 m and only support measures

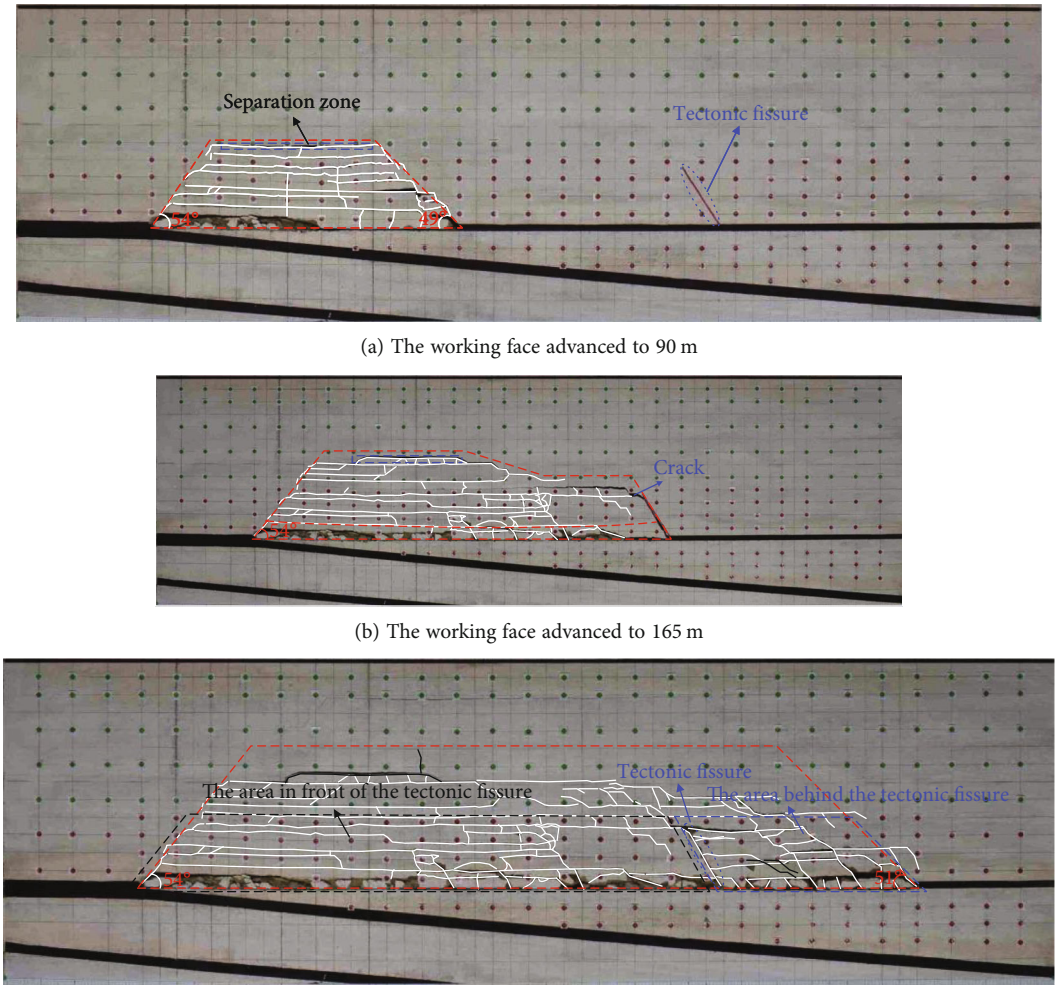

(a) The working face advanced to 90 m

(b) The working face advanced to 165 m

(c) The working face advanced to 220 m

Figure 5: Deformation characteristics of overburden during no. 7-1 coal seam mining.

are taken to strengthen the roof, the broken roof cannot be effectively controlled and the support effect is poor. Under this research background, the Xutuan coal mine attempted to reinforce broken roof by ground grouting. For the ground grouting engineering, the distribution characteristics of porosity and permeability of overburden are the key factors in the design of grouting parameters. The determination of grouting hole position, grouting pressure, single-hole grouting volume, and slurry diffusion radius is all affected by the porosity of overburden.

The volume changes and expansion coefficient of an actively mined rock mass can be determined using the ratio of volume before and after crushing [57, 58]:

$$K_p = \frac{V_h}{V_q}. \tag{2}$$

In formula (2), V_q and V_h are the volume of the rock mass before and after mining.

According to the definition of porosity, the porosity n of broken rock mass due to the mining influence is the ratio of pore volume to total volume of the broken rock mass:

$$n = \frac{V_h - V_q}{V_h} = 1 - \frac{1}{K_p}. \tag{3}$$

Summarizing the previous research results [59, 60], in the similar simulation experiment, with increasing vertical distance from the working face and considering the cumulative effect of the rock mass expansion coefficient, the average rock mass expansion coefficient in different height ranges can be calculated using the following formula:

$$K_p = \frac{V_h}{V_q} = \frac{M + h - \Delta h}{h}. \tag{4}$$

In formula (4), K_p is the expansion coefficient of the rock mass. M is the thickness of the coal seam (unit: m). h is the distance between the roof measuring point and top interface

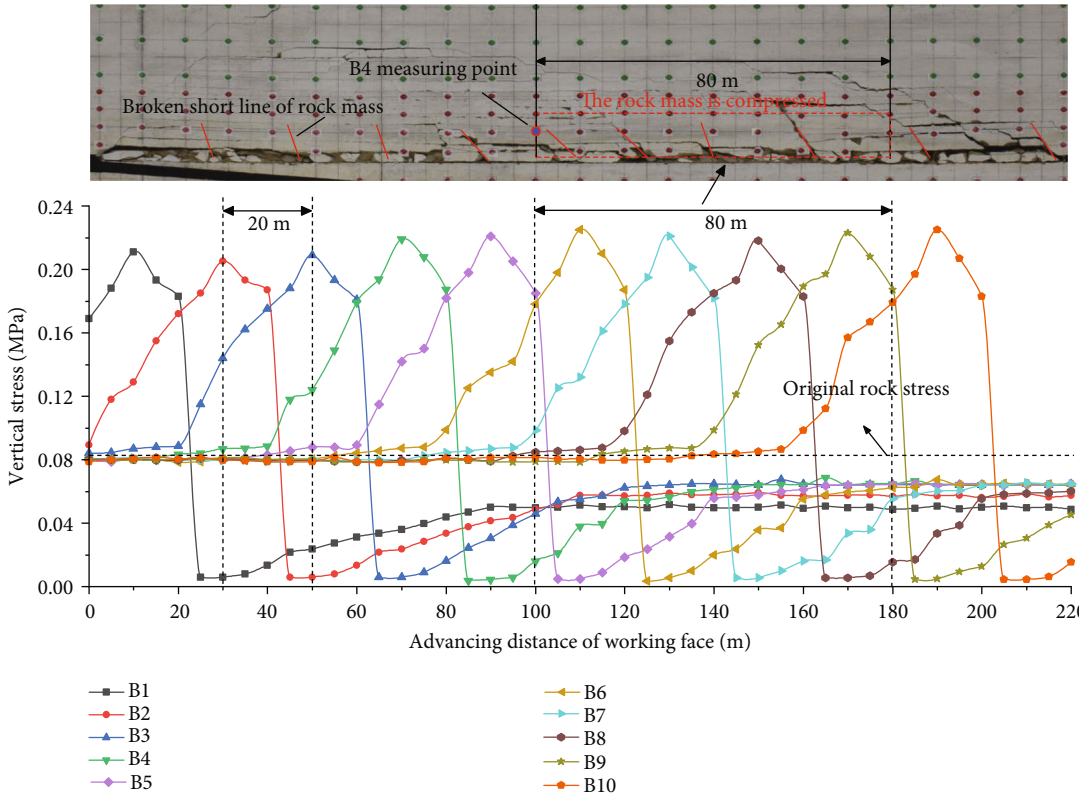

Figure 6: Stress variation diagram of overburden due to the mining influence (B monitoring line).

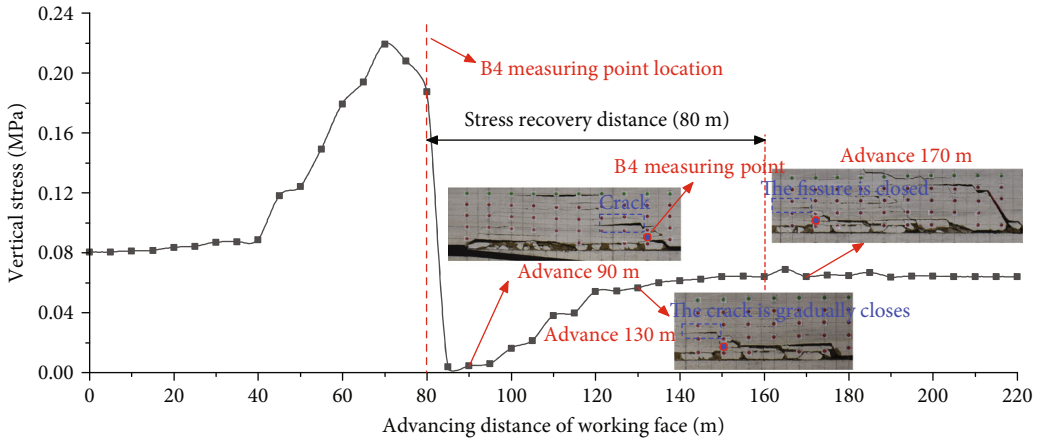

Figure 7: Relationship between stress recovery and dynamic evolution of crack morphology.

of the coal seam (unit: m). Δh is the subsidence of the measuring point (unit: m). The expression of porosity n is

$$n = \frac{V_h - V_q}{V_h} = 1 - \frac{1}{K_p} = 1 - \frac{M + h - \Delta h}{h}. \quad (5)$$

Displacement measuring point data are used in equation (5) to calculate the porosity at different positions in overburden. According to the coordinate values of the measuring points in the model, import origin software to draw the plane porosity cloud map of the model. The distribution characteristics of overburden porosity of the no. 7-1 coal seam when the working face advances to 50 m, 110 m, and 220 m are shown in Figure 14.

When the working face advances to 50 m, the overburden directly collapses and fills the goaf (Figure 14(a)). The maximum porosity of the loose caving zone is 39.5% at the end of the working face and within 3 m of the roof. The sandstone layer at 8 m from the roof has not been broken, the rock deformation is weak, and the change in porosity is small. When the working face advances to 110 m, the support of the cantilever beam structure at the end of the working face hinders downward movement of the upper rock mass. There is a large space

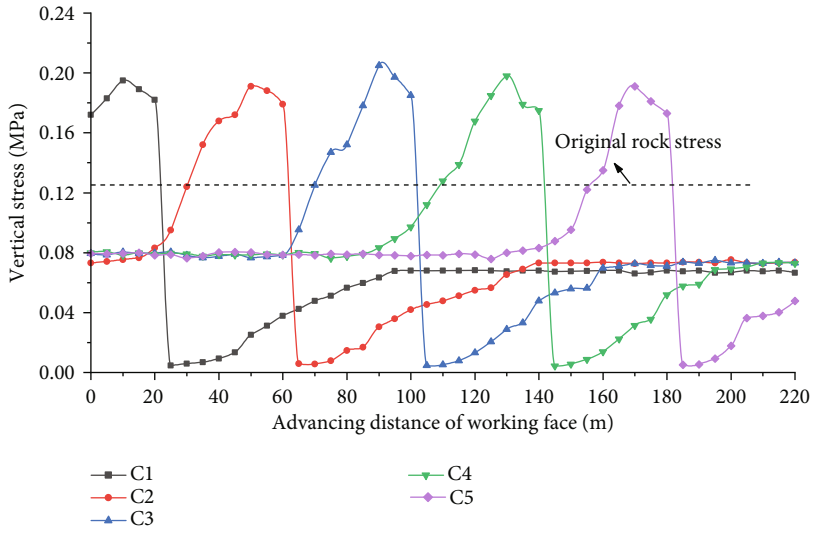

Figure 8: Stress variation diagram of overburden due to the mining influence (C monitoring line).

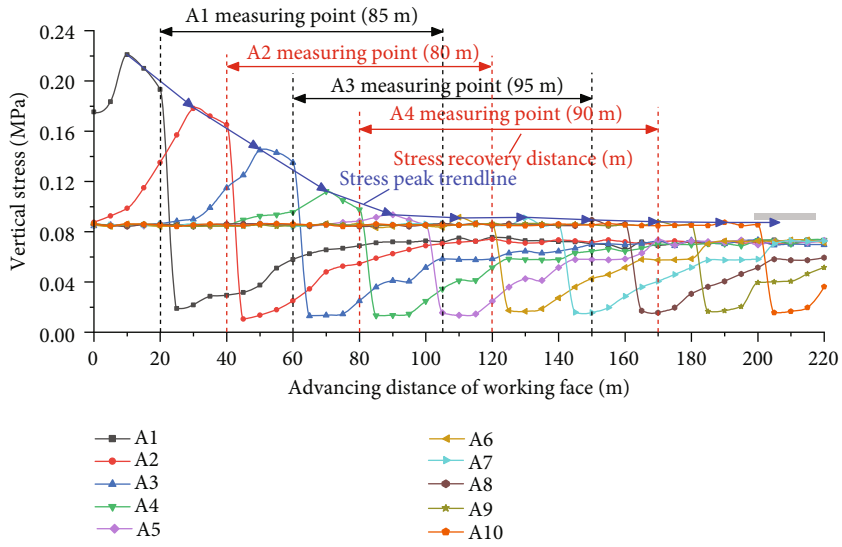

Figure 9: Transfer characteristics of floor stress during mining of the no. 7-1 coal seam.

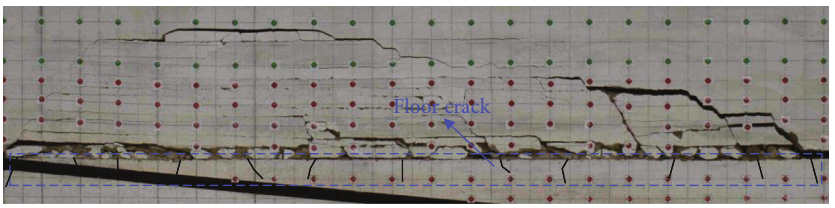

Figure 10: Schematic diagram of floor crack development due to the mining influence.

at the lower part of the cantilever beam, resulting in relatively large porosity of the overburden (Figure 14(b)). Within 8 m of the roof, the maximum porosity is 16.4%, and as the disturbed range of the overburden expands upward, the failure area of overburden increases, and the overburden porosity changes. In the horizontal direction, the maximum porosity of the rock mass in the collapse zone within 40 m of the cut hole is 34.3%, and the minimum porosity is 13.5%. Near the middle of the working face, the rock mass is gradually compacted due to stress recovery, and the porosity is 10%~12%. Vertically, the rock mass above the cut hole is broken upward along the fracture line. Within the separation area near the cut hole, the porosity of the rock mass is 12.0%~34.3%. The area above 33 m from the roof of the working face is relatively less affected by mining, and the porosity of the rock mass is not significantly affected. When the working face is mined to 220 m,

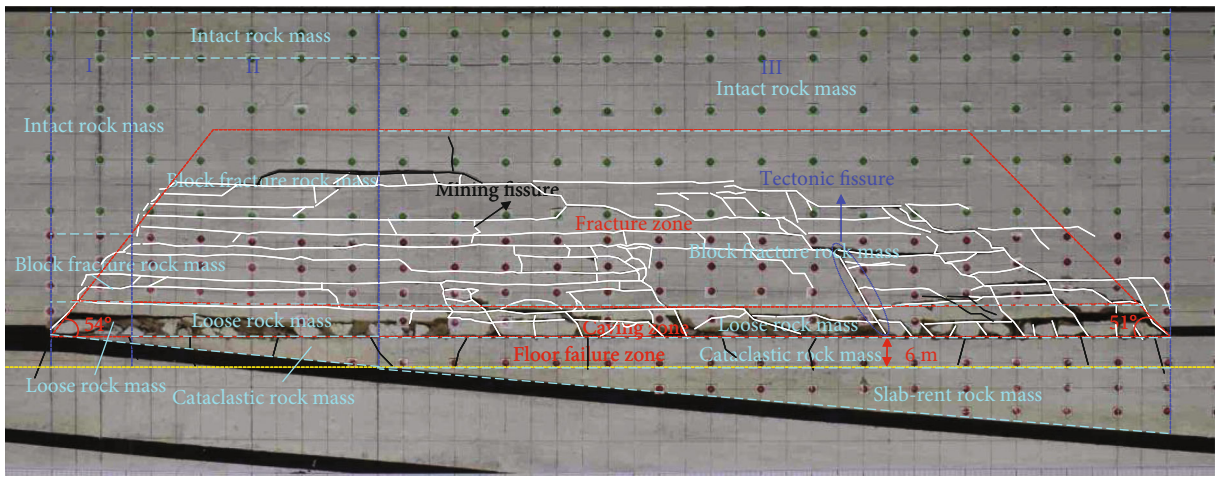

Figure 11: Schematic diagram of overburden structure division due to the mining influence.

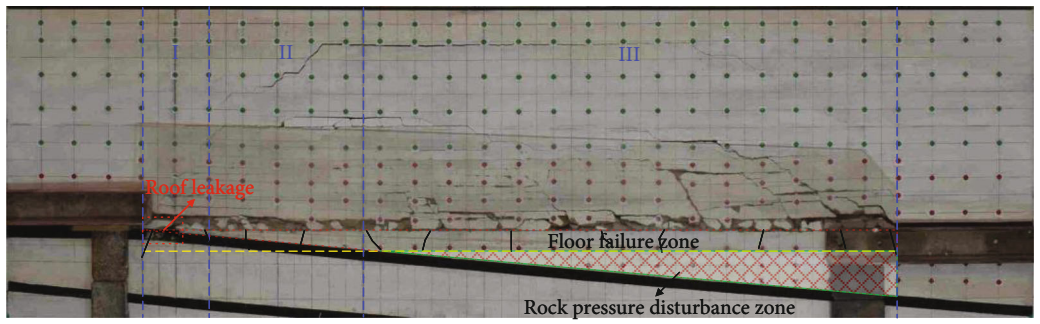

(a) The working face is advanced to 10 m

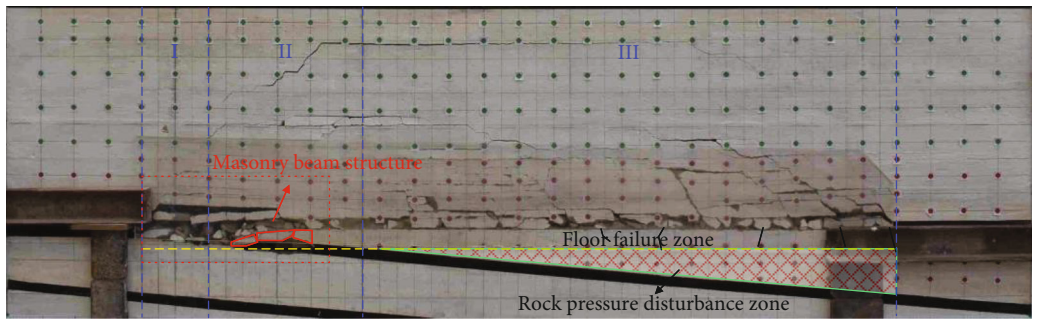

(b) The working face is advanced to 50 m

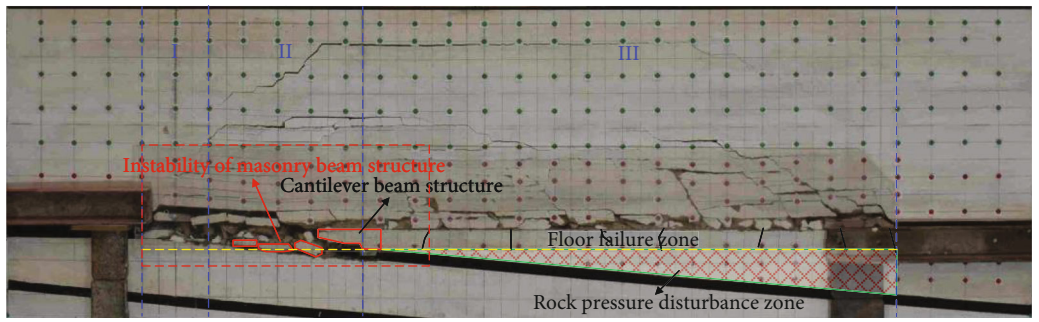

(c) The working face is advanced to 70 m

Figure 12: Schematic diagram of overburden fracture formation during 70 m advancement of the no. 7-2 coal seam.

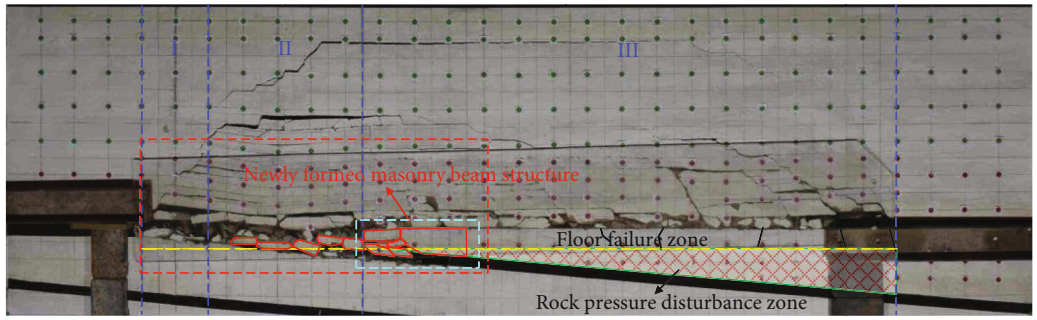

(a) The working face is advanced to 90 m

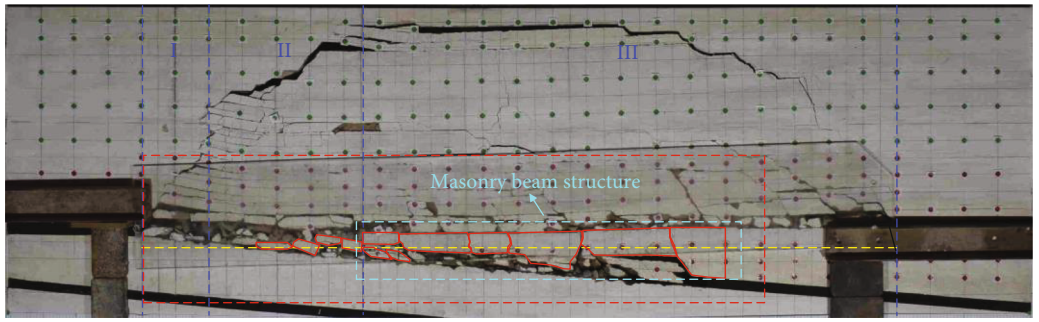

(b) The working face is advanced to 165 m

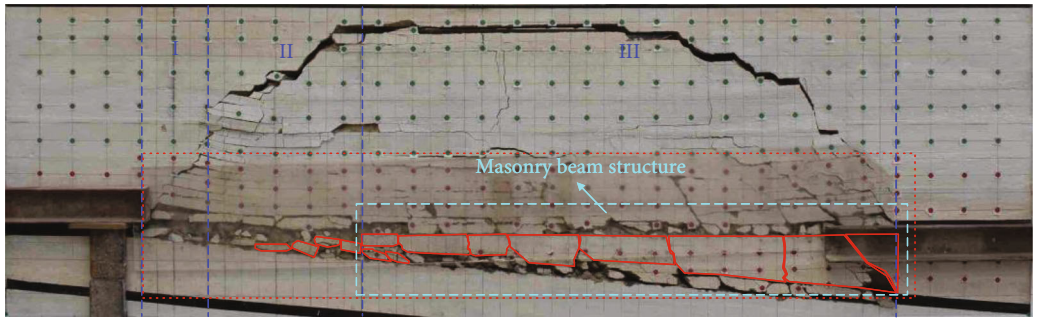

(c) The working face is advanced to 220 m

Figure 13: Schematic diagram of overburden fracture formation during advancement of the no. 7-2 coal seam to 90 m~220 m.

the maximum porosity of the surrounding rock near the cutting hole of the working face is 32.1%, and the maximum porosity of the surrounding rock near the stopping line of the working face is 32.6% (Figure 14(c)). The porosity gradually decreases away from both ends of the goaf to the middle. The middle compaction area ranges from 110 m to 190 m, at which point the porosity of the compaction area tends to be stable and less than 5%. The porosity of rock mass is greater than 5% within 70 m from the cut hole and stopping line. A strong disturbance zone is present within 33 m of the roof, and the porosity changes with movement and fracturing of the overburden. After stress recovery, the rock mass is gradually compacted. When the working face advances to 220 m, the compaction degree of overburden in the middle of goaf is significantly greater than that when the working face advances to 110 m. The porosity of overburden at the cut is affected by the separation space and masonry beam structure, and its influence range is 40 m~50 m in the transverse direction of the roof and 0 m~12 m in the longitudinal direction. The distribution characteristics of the porosity of the surrounding rock at the stopping line are similar to those at the cut hole.

The classic permeability porosity relationship Kozeny-Carman (KC) equation connects permeability K with porosity n. This equation is also widely used as the starting point of many permeability models [61–64]:

$$K = \frac{n^3}{(1-n)^2 cS^2}. \tag{6}$$

In formula (6), c is a constant, and the value is 5. S is the specific surface area. On this basis, the KC equation is further modified, and the permeability coefficient expression is [65, 66]

$$k = \frac{n^3 \rho g}{(1-n)^2 cS^2 \mu} = \frac{n^3 d^2 \rho g}{36c(1-n)^2 \mu}. \tag{7}$$

The equation is commonly used to calculate the permeability coefficient of fluid in stope surrounding rock. In formula (7), k is the permeability coefficient (unit: m/s). n is the

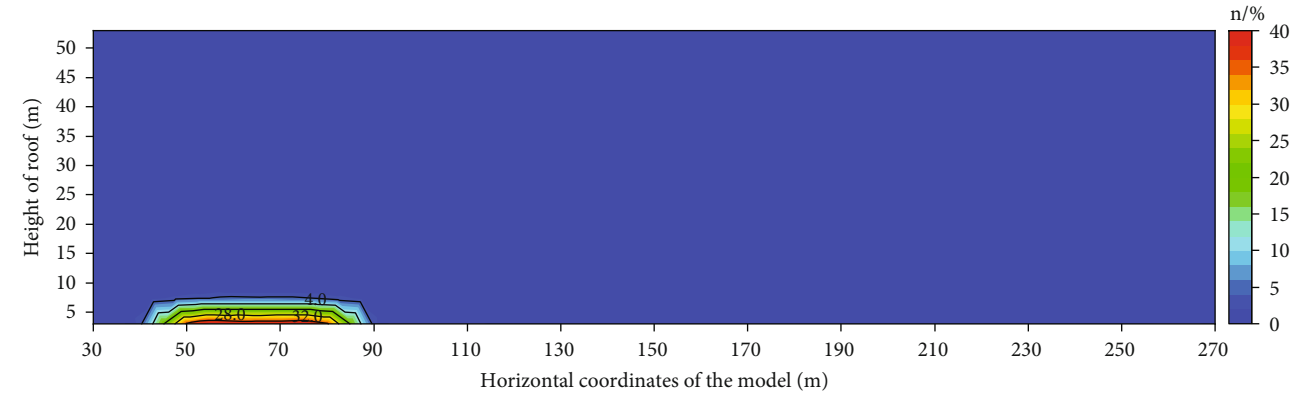

(a) The working face is advanced to 50 m

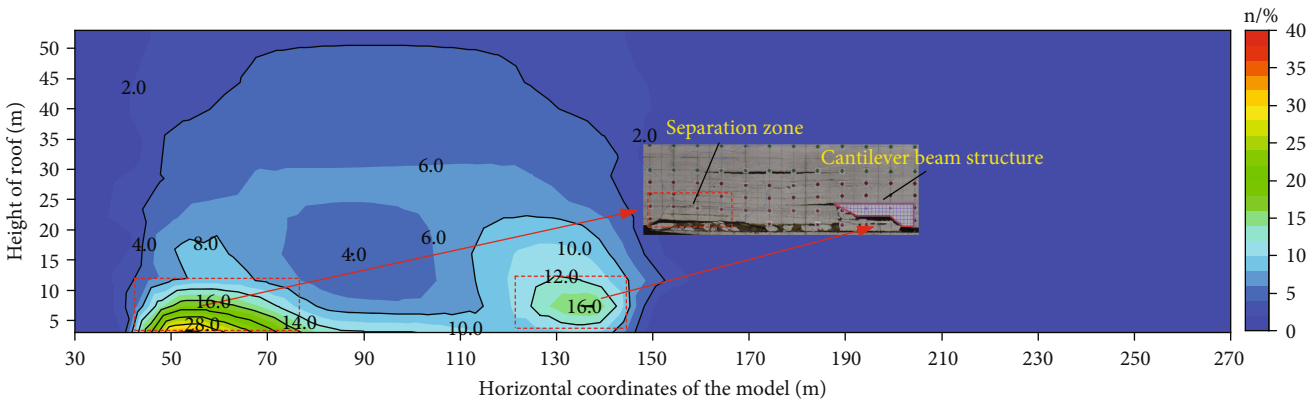

(b) The working face is advanced to 110 m

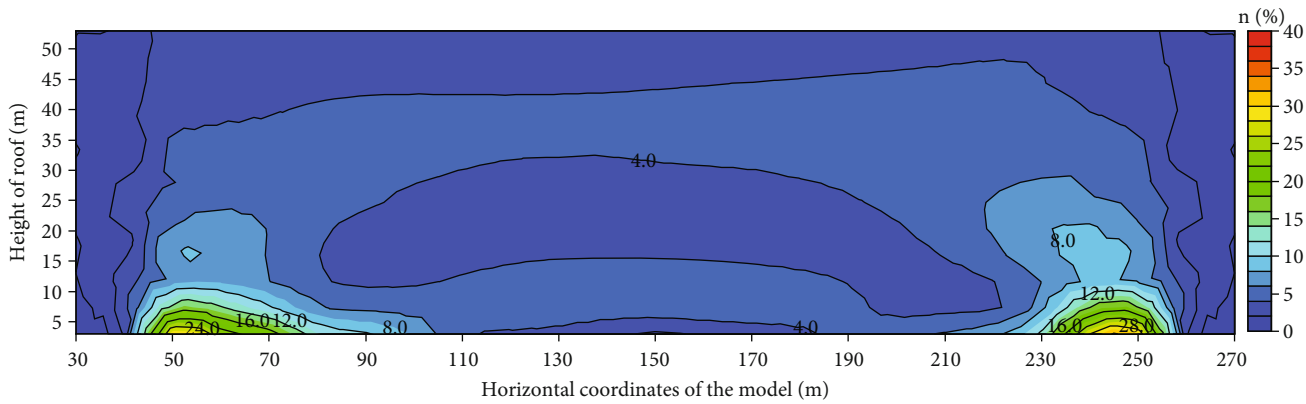

(c) The working face is advanced to 220 m

Figure 14: Distribution of overburden porosity during no. 7-1 coal seam mining.

porosity. d is the average diameter of the fractured rock mass, which is 0.5 m. ρ is the slurry density, with a value of 1309 kg/m^3. μ is the dynamic viscosity coefficient of slurry, which is 9×10^{-3} kg/(m $*$ s); g is the gravitational acceleration, taking 9.8 m/s^2.

The plane distribution law of permeability coefficient of slurry in overburden once mining of the 7-1 coal seam is completed is shown in Figure 15.

4.2. Division of Grouting Difficulty Degree in the Reconstruction Area of Broken Rock Mass with the Regenerated Roof. Based on the porosity difference in two rock mass zones, the surrounding rock at the cut of the caving zone and the stopping line is the primary space for slurry seepage and storage. According to the transverse distribution law of rock porosity and permeability coefficient in the goaf caving zone and the compaction characteristics of caving rock mass in goaf, the difficulty degree of overburden grouting is divided into different regions. The vertical plane of overburden is divided into an extremely easy grouting area, easy grouting area, and difficult grouting area (Figure 15) (Table 3).

(1) In the extremely easy grouting area, the caving rock mass in the goaf does not bear the abutment pressure

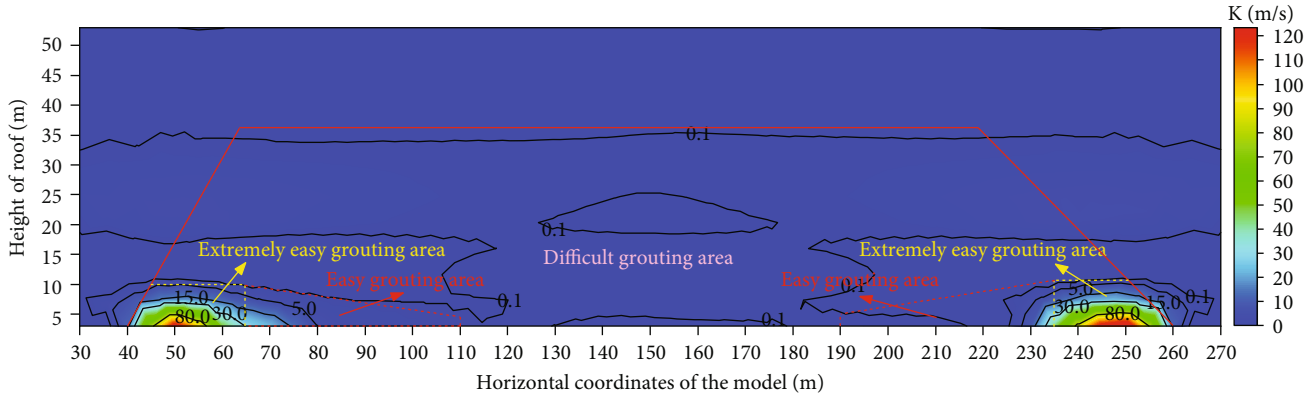

Figure 15: Regional division of grouting difficulty in overburden.

Table 3: Classification of grouting difficulty in overburden due to the mining influence.

Types	Distance from the coal wall (m)	Characteristics of caving rock mass	n (%)	Permeability coefficient (m/s)
Extremely easy grouting area	0 m~25 m	Rocks accumulate naturally	≥20	≥30
Easy grouting area	25 m~70 m	Rocks affected by load	$5 \le n < 20$	$0.1 \le k < 30$
Difficult grouting area	>70 m	The rock was compacted	$n < 5$	<0.1

and forms a natural accumulation state. The porosity of the caving rock mass is $n \ge 20\%$, and the permeability coefficient is $k \ge 30$ m/s. The slurry is flowing easily with this area, and grouting can be completed at low pressure. However, the area and seepage space are small, which are generally distributed on both sides of the coal wall of the roadway as well as within a certain range of the open cut and stopping line

(2) In the easy grouting area, the caving rock mass is under stress due to the action of the masonry beam structure of the overlying strata, and the caving rock mass is gradually compacted with increasing roof subsidence. The porosity range of the collapsed rock mass is $5\% \le n \le 20\%$, and the permeability coefficient is $0.1 \le k \le 30$ m/s

(3) In the difficult grouting area, the abutment pressure values in each area are relatively similar, and the caving rock mass is fully compacted and is stable. The porosity of the caving rock mass is $n < 5\%$, and the permeability coefficient is $k < 0.1$ m/s. The rock mass in this area requires grouting under high grouting pressure and is generally located in the central compaction area of the goaf

5. Conclusion

This paper reveals the structural characteristics of the regenerated roof of the lower coal seam after the mining of the upper coal seam in the bifurcated coal seam through the similar simulation test, divides the roof structure into types, and analyzes the stability of the roof of different structural types. Mining practice and similar simulation test results show that when the spacing of bifurcated coal seams is less than 6 m, the roof of the lower coal seam is relatively broken after mining of the upper coal seam, and a variety of support measures are taken, which is still difficult to control in the mining process of the lower coal seam. Under this background, the author studies the porosity and permeability characteristics of overburden under the mining influence of the upper coal seam and obtains the distribution law of porosity and permeability of overburden. The research results can provide reference for the parameter design of the ground grouting engineering of the regenerated roof. The main conclusions are as follows:

(1) After mining of the upper coal seam, the surrounding rock structure changes. Affected by interlayer distance, structural types of the regenerated roof of the lower coal seam can be primarily divided into three types from top to bottom, namely: intact rock mass+block fracture rock mass+loose rock mass (type I structure); intact rock mass+block fracture rock mass+loose rock mass+cataclastic rock mass (type II structure); and intact rock mass+block fracture rock mass+loose rock mass+cataclastic rock mass+slab-rent rock mass (type III structure)

(2) Through mining of the lower coal seam, the stability of three kinds of recycled roof structures is evaluated. Based on overburden migration and fracturing during mining of the lower coal seam, the stability of the three kinds of recycled roof structures is obtained: III > II > I

(3) Differences in porosity and permeability characteristics of overburden after mining of the upper coal

seam are analyzed. The porosity of the goaf and overburden at the cut hole and stopping line is significantly larger than that in the middle compaction area. Within 70 m of the coal wall, the rock mass porosity is greater than 5%, and the permeability coefficient of slurry in this range is greater than 0.1 m/s

(4) Based on porosity and permeability differences in the overburden, the difficulty degree of overburden grouting is divided into three areas: extremely easy grouting area, easy grouting area, and difficult grouting area

Data Availability

The data used for calculation in this paper can be obtained from the author.

Conflicts of Interest

The authors declare that they have no conflicts of interest.

Acknowledgments

The authors are grateful for the financial support provided by the Innovation Team Construction Project of University Scientific Research Platform in Anhui Province (2016-2018-24), the Anhui Province Natural Science Foundation (2008085QE226), and the National Natural Science Foundation of China (Grant nos. 41272278 and 52104117). We thank the School of Mining Engineering of Anhui University of Science and Technology for providing the site for this similar simulation test and thank the experimenter Bao Ming for his help in the process of the experiment. Finally, we would like to thank the authors of the references cited in this paper for their contributions in the field of mining.

References

[1] D. Y. Hao, Y. Z. Wu, H. J. Chen, X. W. Chu, and Y. Li, "Instability mechanism and prevention technology of roadway in close distance and extra thick coal seam under goaf," *Journal of China Coal Society*, vol. 44, no. 9, pp. 2682–2690, 2019.

[2] G. Y. Peng, M. Z. Gao, Y. C. Lv, and R. G. Zhang, "Investigation on mining mechanics behavior of deep close distance seam group," *Journal of China Coal Society*, vol. 44, no. 7, pp. 1971–1980, 2019.

[3] C. Y. Liu, J. X. Yang, B. Yu, and P. J. Yang, "Destabilization regularity of hard thick roof group under the multi gob," *Journal of China Coal Society*, vol. 39, no. 3, pp. 395–403, 2014.

[4] H. P. Kang, Z. Zhang, and Z. Z. Huang, "Characteristics of roof disasters and controlling techniques of coal mine in China," *Safety in Coal Mines*, vol. 51, no. 10, pp. 24–33, 2020.

[5] H. P. Kang, "Seventy years development and prospects of strata control technologies for coal mine roadways in China," *Chinese Journal of Rock Mechanics and Engineering*, vol. 40, no. 1, pp. 1–30, 2021.

[6] W. D. Wu, J. B. Bai, X. Y. Wang, Z. J. Zhu, and S. Yan, "Field investigation of fractures evolution in overlying strata caused by extraction of the Jurassic and Carboniferous coal seams and its application: case study," *International Journal of Coal Geology*, vol. 208, pp. 12–23, 2019.

[7] F. Cui, C. Jia, and X. P. Lai, "Study on deformation and energy release characteristics of overlying strata under different mining sequence in close coal seam group based on similar material simulation," *Energies*, vol. 12, no. 23, p. 4485, 2019.

[8] W. H. Sui, Y. Hang, L. X. Ma et al., "Interactions of overburden failure zones due to multiple-seam mining using longwall caving," *Bulletin of Engineering Geology and the Environment*, vol. 74, no. 3, pp. 1019–1035, 2015.

[9] J. Lu, C. B. Jiang, Z. Jin, W. Wang, W. Zhuang, and H. Yu, "Three-dimensional physical model experiment of mining-induced deformation and failure characteristics of roof and floor in deep underground coal seams," *Process Safety and Environmental Protection*, vol. 150, pp. 400–415, 2021.

[10] J. Wang, P. Q. Qiu, J. G. Ning, L. Zhuang, and S. Yang, "A numerical study of the mining-induced energy redistribution in a coal seam adjacent to an extracted coal panel during longwall face mining: a case study," *Energy Science & Engineering*, vol. 8, no. 3, pp. 817–835, 2020.

[11] H. Yan, M. Y. Weng, R. M. Feng, and W. K. Li, "Layout and support design of a coal roadway in ultra-close multiple-seams," *Journal of Central South University*, vol. 22, no. 11, pp. 4385–4395, 2015.

[12] X. J. Liu, X. M. Li, and W. D. Pan, "Analysis on the floor stress distribution and roadway position in the close distance coal seams," *Arabian Journal of Geosciences*, vol. 9, no. 2, pp. 4385–4395, 2016.

[13] W. Zhang, D. S. Zhang, D. H. Qi, W. Hu, Z. He, and W. Zhang, "Floor failure depth of upper coal seam during close coal seams mining and its novel detection method," *Energy Exploration & Exploitation*, vol. 36, no. 5, pp. 1265–1278, 2018.

[14] X. M. Sun, Y. Y. Liu, J. W. Wang, J. Li, S. Sun, and X. Cui, "Study on three-dimensional stress field of gob-side entry retaining by roof cutting without pillar under near-group coal seam mining," *PRO*, vol. 7, no. 9, p. 552, 2019.

[15] H. F. Shang, J. G. Ning, S. C. Hu, S. Yang, and P. Qiu, "Field and numerical investigations of gateroad system failure under an irregular residual coal pillar in close-distance coal seams," *Energy Science & Engineering*, vol. 7, no. 6, pp. 2720–2740, 2019.

[16] Y. Xiong, D. Z. Kong, Z. B. Cheng et al., "Instability control of roadway surrounding rock in close-distance coal seam groups under repeated mining," *Energies*, vol. 14, no. 16, p. 5193, 2021.

[17] Z. Y. Sun, Y. Z. Wu, Z. G. Lu, Y. Feng, X. Chu, and K. Yi, "Stability analysis and derived control measures for rock surrounding a roadway in a lower coal seam under concentrated stress of a coal pillar," *Shock and Vibration*, vol. 2020, Article ID 6624983, 12 pages, 2020.

[18] X. Gao, S. Zhang, Y. Zi, and S. K. Pathan, "Study on optimum layout of roadway in close coal seam," *Arabian Journal of Geosciences*, vol. 13, no. 15, 2020.

[19] Y. L. Xu, K. R. Pan, and H. Zhang, "Investigation of key techniques on floor roadway support under the impacts of superimposed mining: theoretical analysis and field study," *Environmental Earth Sciences*, vol. 78, no. 15, 2019.

[20] W. K. Ru, S. C. Hu, J. G. Ning et al., "Study on the rheological failure mechanism of weakly cemented soft rock roadway during the mining of close-distance coal seams: a case study," *Advances in Civil Engineering*, vol. 2020, Article ID 8885849, 20 pages, 2020.

[21] Y. L. Huang, J. X. Zhang, W. Yin, and Q. Sun, "Analysis of overlying strata movement and behaviors in caving and solid backfilling mixed coal mining," *Energies*, vol. 10, no. 7, p. 1057, 2017.

[22] K. Gao, P. Huang, Z. G. Liu, J. Liu, F. Wang, and C. M. Shu, "Pressure relief by blasting roof cutting in close seam group mining under thick sandstone to enhance gas extraction for mining safety," *PRO*, vol. 9, no. 4, p. 603, 2021.

[23] Q. H. Huang, Y. P. He, and L. B. Luo, "Study on the active structure of caved roof and support resistance in shallow buried and ultra-close coal seams mining," *Journal of Mining & Safety Engineering*, vol. 35, no. 3, pp. 561–566, 2018.

[24] Y. T. Sun, G. C. Li, N. Zhang, Q. Chang, J. Xu, and J. Zhang, "Development of ensemble learning models to evaluate the strength of coal-grout materials," *International Journal of Mining Science and Technology*, vol. 31, no. 2, pp. 153–162, 2021.

[25] D. Z. Kong, Z. B. Cheng, and S. S. Zheng, "Study on the failure mechanism and stability control measures in a large-cutting-height coal mining face with a deep-buried seam," *Bulletin of Engineering Geology and the Environment*, vol. 78, no. 8, pp. 6143–6157, 2019.

[26] K. Wang, L. G. Wang, and B. Ren, "Failure mechanism analysis and support technology for roadway tunnel in fault fracture zone: a case study," *Energies*, vol. 14, no. 13, p. 3767, 2021.

[27] J. P. Zhang, L. M. Liu, Q. H. Li et al., "Development of cement-based self-stress composite grouting material for reinforcing rock mass and engineering application," *Construction and Building Materials*, vol. 201, pp. 314–327, 2019.

[28] D. Y. Qian, N. Zhang, M. W. Zhang et al., "Application and evaluation of ground surface pre-grouting reinforcement for 800-m-deep underground opening through large fault zones," *Arabian Journal of Geosciences*, vol. 10, no. 13, 2017.

[29] Q. Wang, H. K. Gao, H. C. Yu, B. Jiang, and B. H. Liu, "Method for measuring rock mass characteristics and evaluating the grouting-reinforced effect based on digital drilling," *Rock Mechanics and Rock Engineering*, vol. 52, no. 3, pp. 841–851, 2019.

[30] D. P. Adhikary and H. Guo, "Modelling of longwall mining-induced strata permeability change," *Rock Mechanics and Rock Engineering*, vol. 48, no. 1, pp. 345–359, 2015.

[31] C. Zhang, S. H. Tu, and Y. X. Zhao, "Compaction characteristics of the caving zone in a longwall goaf: a review," *Environmental Earth Sciences*, vol. 78, no. 1, 2019.

[32] B. A. Poulsen, D. P. Adhikary, and H. Guo, "Simulating mining-induced strata permeability changes," *Rock Mechanics and Rock Engineering*, vol. 237, pp. 208–216, 2018.

[33] H. Wu and D. Ma, "Fracture phenomena and mechanisms of brittle rock with different numbers of openings under uniaxial loading," *Geomechanics and Engineering*, vol. 25, no. 6, pp. 481–493, 2021.

[34] D. Ma, J. J. Wang, X. Cai et al., "Effects of height/diameter ratio on failure and damage properties of granite under coupled bending and splitting deformation," *Engineering Fracture Mechanics*, vol. 220, p. 106640, 2019.

[35] D. Ma, J. X. Zhang, H. Y. Duan et al., "Reutilization of gangue wastes in underground backfilling mining: overburden aquifer protection," *Chemosphere*, vol. 264, no. 1, 2021.

[36] D. Ma, S. B. Kong, Z. H. Li, Q. Zhang, Z. Wang, and Z. Zhou, "Effect of wetting-drying cycle on hydraulic and mechanical properties of cemented paste backfill of the recycled solid wastes," *Chemosphere*, vol. 282, p. 131163, 2021.

[37] S. F. Wang, X. B. Li, and D. M. Wang, "Void fraction distribution in overburden disturbed by longwall mining of coal," *Environmental Earth Sciences*, vol. 75, no. 2, 2016.

[38] G. Y. Si, J. Q. Shi, S. Durucan et al., "Monitoring and modelling of gas dynamics in multi-level longwall top coal caving of ultra-thick coal seams, part II: numerical modelling," *International Journal of Coal Geology*, vol. 144-145, pp. 58–70, 2015.

[39] Z. P. Meng, X. C. Shi, and G. Q. Li, "Deformation, failure and permeability of coal-bearing strata during longwall mining," *Rock Mechanics and Rock Engineering*, vol. 208, pp. 69–80, 2016.

[40] R. Hu, J. W. Wu, W. B. Shi, X. Zhai, and K. Huang, "Study on evolution characteristics of regenerated roof structure in downward mining of bifurcated coal seam," *Advances in Materials Science and Engineering*, vol. 2021, Article ID 8226616, 13 pages, 2021.

[41] J. Chai, W. G. Du, Q. Yuan, and D. Zhang, "Analysis of test method for physical model test of mining based on optical fiber sensing technology detection," *Optical Fiber Technology*, vol. 48, pp. 84–94, 2019.

[42] G. W. Cheng, T. H. Yang, H. Y. Liu et al., "Characteristics of stratum movement induced by downward longwall mining activities in middle-distance multi-seam," *International Journal of Rock Mechanics and Mining Sciences*, vol. 136, p. 104517, 2020.

[43] W. T. Liu, L. F. Pang, B. C. Xu, and X. Sun, "Study on overburden failure characteristics in deep thick loose seam and thick coal seam mining," *Geomatics, Natural Hazards and Risk*, vol. 11, no. 1, pp. 632–653, 2020.

[44] T. Hu, G. Y. Hou, and Z. X. Li, "The field monitoring experiment of the roof strata movement in coal mining based on DFOS," *Sensors*, vol. 20, no. 5, p. 1318, 2020.

[45] J. J. Li, F. J. Li, M. S. Hu, X. Zhou, and Y. Huo, "Dynamic monitoring of the mining-induced fractured zone in overburden strata, based on geo-electrical characteristics," *Arabian Journal of Geosciences*, vol. 12, no. 14, 2019.

[46] J. G. Ning, J. Wang, Y. L. Tan, and Q. Xu, "Mechanical mechanism of overlying strata breaking and development of fractured zone during close-distance coal seam group mining," *International Journal of Mining Science and Technology*, vol. 30, no. 2, pp. 207–215, 2020.

[47] G. W. Cheng, T. H. Ma, C. A. Tang, H. Liu, and S. Wang, "A zoning model for coal mining-induced strata movement based on microseismic monitoring," *International Journal of Rock Mechanics and Mining Sciences*, vol. 94, pp. 123–138, 2017.

[48] W. Guo, G. Zhao, G. Lou, and S. Wang, "A new method of predicting the height of the fractured water-conducting zone due to high-intensity longwall coal mining in China," *Rock Mechanics and Rock Engineering*, vol. 52, no. 8, pp. 2789–2802, 2019.

[49] W. Y. Lu, C. C. He, and X. Zhang, "Height of overburden fracture based on key strata theory in longwall face," *PLoS One*, vol. 15, no. 1, 2020.

[50] T. Hu, G. Y. Hou, S. Bu et al., "A novel approach for predicting the height of water-conducting fracture zone under the high overburden caving strength based on optimized processes," *Process*, vol. 8, no. 8, p. 950, 2020.

[51] Y. P. Liang, B. Li, and Q. L. Zou, "Movement type of the first subordinate key stratum and its influence on strata behavior

in the fully mechanized face with large mining height," *Arabian Journal of Geosciences*, vol. 12, no. 2, 2019.

[52] Z. C. Ren and N. Wang, "The overburden strata caving characteristics and height determination of water conducting fracture zone in fully mechanized caving mining of extra thick coal seam," *Geotechnical and Geological Engineering*, vol. 38, no. 1, pp. 329–341, 2020.

[53] X. L. Wang, Q. R. Qin, and C. H. Fan, "Failure characteristic and fracture evolution law of overburden of thick coal in fully mechanized sub-level caving mining," *Journal of Engineering Geology*, vol. 46, no. 11, pp. 2041–2048, 2017.

[54] W. H. Sui, D. Y. Zhang, Z. C. Cui, Z. Wu, and Q. Zhao, "Environmental implications of mitigating overburden failure and subsidences using paste-like backfill mining: a case study," *International Journal of Mining, Reclamation and Environment*, vol. 29, no. 6, pp. 521–543, 2015.

[55] Q. X. Huang and J. B. Han, "Study on fracture evolution mechanism of shallow-buried close coal seam mining," *Journal of Mining & Safety Engineering*, vol. 36, no. 4, pp. 706–711, 2019.

[56] H. Z. Wang, Y. J. Ju, and K. K. Qin, "A comparative study on floor failure law in deep and short-distance coal seam mining," *Journal of Mining & Safety Engineering*, vol. 37, no. 3, pp. 553–560, 2020.

[57] C. D. Su, M. Gu, X. Tang, and W. B. Guo, "Experiment study of compaction characteristics of crushed stones from coal seam roof," *Chinese Journal of Rock Mechanics and Engineering*, vol. 31, no. 1, pp. 18–26, 2012.

[58] B. F. Wang, B. Liang, J. G. Wang, K. M. Sun, and H. B. Chi, "Experiment study on rock bulking of coal mine underground reservoir," *Rock and Soil Mechanics*, vol. 39, no. 11, pp. 4086–4092, 2018.

[59] K. Z. Deng, M. Zhou, and Z. X. Tan, "Study on laws of rock mass breaking induced by mining," *Journal of China University of Mining and Technology*, vol. 27, no. 3, pp. 261–264, 1998.

[60] L. H. Sun, H. G. Ji, H. Jiang, P. Zeng, and B. S. Yang, "Experimental study on characteristics of broken caving and regularity of compaction deformation of rocks in caving zone in the weakly cemented strata," *Journal of China Coal Society*, vol. 42, no. 10, pp. 2565–2572, 2017.

[61] P. C. Carman, "Permeability of saturated sands, soils and clays," *The Journal of Agricultural Science*, vol. 29, no. 2, pp. 262–273, 1939.

[62] P. C. Carman, "Book reviews: flow of gases through porous media," *Science*, vol. 124, pp. 1254-1255, 1956.

[63] J. Kozeny, "Ueber kapillare leitung des wassers im boden," *Sitzungsberichte der Kaiserlichen Akademie der Wissenschaften in Wien*, vol. 136, pp. 271–306, 1927.

[64] P. Xu and B. M. Yu, "Developing a new form of permeability and Kozeny-Carman constant for homogeneous porous media by means of fractal geometry," *Advances in Water Resources*, vol. 31, no. 1, pp. 74–81, 2008.

[65] J. Bear and B. M. Yu, *Dynamics of Fluid in Porous Media*, Elsevier, New York, 1972.

[66] M. Kaviany, *Principles of Heat Transfer in Porous Media*, Springer, New York, 1995.